CORA Cork Open Research Archive
Cartlann Taighde Oscailte Chorcaí

Title	Structural and optical properties of post-annealed atomic-layer-deposited HfO2 thin films on GaAs
Authors	Bennett, N.S.;Cherkaoui, Karim;Wong, C. S.;O'Connor, Éamon;Monaghan, Scott;Hurley, Paul K.;Chauhan, L.;McNally, P. J.
Publication date	2014-08-29
Original Citation	Bennett, N. S., Cherkaoui, K., Wong, C. S., O'Connor, É., Monaghan, S., Hurley, P., Chauhan, L. and McNally, P. J. (2014) 'Structural and optical properties of post-annealed atomic-layer-deposited HfO2 thin films on GaAs', Thin Solid Films, 569, pp. 104-112. doi: 10.1016/j.tsf.2014.08.025
Type of publication	Article (peer-reviewed)
Link to publisher's version	10.1016/j.tsf.2014.08.025
Rights	© 2014, Elsevier B.V. All rights reserved. This manuscript version is made available under the CC BY-NC-ND 4.0 license. - https://creativecommons.org/licenses/by-nc-nd/4.0/
Download date	2024-04-25 04:02:26
Item downloaded from	https://hdl.handle.net/10468/13328

UCC
University College Cork, Ireland
Coláiste na hOllscoile Corcaigh

*Manuscript
Click here to view linked References

Structural and Optical Properties of Post-Annealed Atomic-Layer-Deposited HfO_2 Thin Films on GaAs

N. S. Bennett[1*#], K. Cherakoui[2], C. S. Wong[1], É. O'Connor[2], S. Monaghan[2], P. Hurley[2], L. Chauhan[3] and P. J. McNally[1]

[1] Nanomaterials Processing Lab., School of Electronic Engineering, Dublin City University, Dublin 9, Ireland
[2] Tyndall National Institute, University College Cork, Lee Maltings, Prospect Row, Cork, Ireland
[3] School of Physical Sciences, Dublin City University, Dublin 9, Ireland

*n.bennett@hw.ac.uk, +44 131 451 4379
[#]Now at the Institute of Mechanical, Process and Energy Engineering, School of Engineering and Physical Science, Heriot-Watt University, Edinburgh EH14 4AS, United Kingdom

Abstract

The effects of post-annealing conditions on solid-phase crystallization of atomic-layer-deposited HfO_2 films grown on GaAs were investigated. Film properties, including cystallinity (preferential crystal orientation and crystallite size), thickness, density, permittivity, optical band gap and chemical composition, were monitored as a function of annealing conditions. Following rapid thermal processing (RTP) in nitrogen ambient at temperatures from 325°C to 625°C, the initially produced amorphous/partially crystallized HfO_2 films changed into a well-ordered crystalline structure with no detectable interfacial layer between the film and the GaAs substrate. Though HfO_2 properties were predictable and similar to those of HfO_2 on Si for low temperature processing, in the case of annealing at ≥475°C, the thickness of the film was relatively increased compared to that of an as-grown film and displayed unexpected film characteristics. Changes after annealing in the depth profile data related to stoichiometry indicated that As oxide is formed within the HfO_2 film during the RTP. The formation of As oxide in the HfO_2 film, resulting from the underlying substrate, is dissimilar to previously published results which reported the presence of Ga oxide.

Introduction

The arrival of high-permittivity (high-κ) gate dielectrics into modern transistors marked a paradigm shift in CMOS manufacturing. High-κ dielectrics offer the advantage that a physically thicker gate oxide can be used than if the more traditional SiO_2 gate dielectric were employed. The thicker high-κ film prevents direct tunneling of charge carriers through the dielectric, reducing power dissipation. Hafnium-based oxides, such as hafnium dioxide (HfO_2), with a dielectric constant of $\kappa \sim 20$, have been shown as some of the better performing dielectrics [1].

A further paradigm shift on the horizon for CMOS manufacturers is the introduction of non-Si channels. Given their improved carrier mobility – particularly for electrons – III-V semiconductors are a likely successor to Si and therefore research studies on the compatibility between high-κ dielectrics and III-V semiconductors are essential.

This study focusses on the structural and optical properties of atomic-layer-deposited HfO_2 on the III-V material GaAs, undergoing solid-phase crystallization. Properties are investigated as a function of film thickness and post-annealing temperature and time, all of which are factors that have direct relevance to industrial semiconductor processing. While amorphous, as-deposited HfO_2 has been shown to demonstrate reasonable dielectric performance [2], deliberately or indirectly, hafnia films are often exposed to elevated thermal budgets during post-processing. This exposure to heat can affect fundamental properties of the gate oxide, including film crystallinity, density, band gap and κ value. Here we investigated this behavior for annealing times from seconds up to 6 hours and temperatures in the range 250°C to 625°C. This experimental range is complementary to previous studies that have focused on higher post-annealing temperatures (≥600°C). Comparisons and contrasts with previous findings are discussed.

Experimental

Samples were fabricated from three commercially available 2-inch diameter GaAs (100) wafers of thickness 350µm. N-type GaAs epilayers (400nm thick) were grown by metal-organic vapor-phase epitaxy (MOVPE). The wafers were loaded into sealed nitrogen bags using a nitrogen glove box attached to the MOVPE system. The wafers were then transferred to an atomic-layer deposition (ALD) chamber with minimum exposure to air (less than one minute) before high-κ deposition. The surface received no chemical treatment prior to high-κ film formation. ALD was then carried out in a Cambridge NanoTech system at 250°C to deposit HfO_2 thin films of thickness 5nm, 10nm or 20nm. The Hf ALD precursor used was TEMAHf ($Hf(N(C_2H_5)(CH_3))_4$) in combination with H_2O. Following ALD, the wafers were diced into four pieces. For each wafer one of the pieces was left as-grown, a second piece was annealed in N_2 at 325°C for 60s, the third piece was annealed at 400°C and the fourth piece at 475°C. After the full range of measurements was carried out on the as-grown quarter, it was diced into several smaller pieces and studied by X-ray diffraction with *in situ* annealing, extending the temperature study to higher temperatures and longer annealing times.

A range of characterization techniques was applied to the samples – one being cross-sectional transmission electron microscopy (XTEM). Cross-sections were prepared using an FEI Quanta 200i dual-beam focused ion beam. Three layers were deposited to protect the top surface during milling (SiO_2 at 5kV, 6.6nA; electron beam W at 5kV, 13nA; ion beam Pt at 30kV, 0.5nA). Cross-sections were thinned at 30kV and 100pA with further polishing at 5kV and 48pA. Finally, samples were imaged using a JEOL 2011 TEM using a Gatan double tilt holder. Fast Fourier Transform (FFT) analysis was carried out on each XTEM micrograph using ImageJ software [3] in order to identify preferential crystal growth orientations.

Grazing incidence X-ray diffraction (XRD) was carried out using a Jordan Valley Bede D1 high-resolution X-ray diffractometer. An incident X-ray grazing angle (ω) of 0.5° was employed. The X-ray detector was scanned in the 2theta (2θ) direction from 20° to 80°. A subset of samples was studied by XRD using *in situ* annealing carried out on an Anton Paar DHS1100 domed heater stage. As-deposited samples were annealed at one temperature, being either 325°C, 400°C, 475°C, 550°C, or 625°C, and held at that set temperature for times between 1 min and 6 hrs. Numerous 2θ XRD scans

were carried out in the range 27^{o}-30^{o} to capture changes in the -1 1 1 monoclinic HfO_2 diffraction peak as a function of annealing time.

The same diffractometer was used for X-ray reflectivity (XRR) measurements. *Omega-2theta* (ω–2θ) scans in the range 0 to 7000 arcsec were carried out to investigate thickness and density of the thin films. These parameters were extracted by deriving an optimized model for the sample structure using Bede Refs software [4]. To complement these measurements spectroscopic ellipsometry (SE) was employed using a J.A. Woollam ellipsometer to investigate the refractive index and optical band gap of the samples.

X-ray photoelectron spectroscopy (XPS) analysis was carried out using a VG Microtech electron spectrometer at a base pressure of 10^{-9} mbar. Photoelectrons are excited with a conventional Al Kα = 1486.6 eV X-ray source and a VG CLAM electron energy analyzer operating at a 20 eV pass energy. All spectrum binding energies were referenced to the hydrocarbon C 1s peak at 285 eV to correct for electrostatic charging effects during acquisition.

Finally, ultra-low energy (300 eV) secondary-ion mass spectrometry (SIMS) was carried out on selected samples to look at the atomic depth profile of elements in the thin film and substrate using an incident beam of either O_2^+ or Cs^+ ions. In each case the beam scan area was 300x300 μm, however only the central 100x100 μm was analyzed to avoid ion contamination caused by sputtering of the crater walls.

Results

i) Crystallinity

XTEM micrographs in Fig. 1 demonstrate two quite distinct layers at the sample surfaces representing GaAs and HfO_2 and each film thickness appears to correlate closely with the nominal thickness specified during ALD. In all cases there is little evidence of any interlayer, with bright layers at the interface resulting from imaging conditions. Starting with the 5nm as-deposited film (far left in Fig. 1a), the HfO_2 film shows little evidence of crystal structure and appears to be amorphous. Interestingly, crystallinity appears dependent on film thickness, with increasing appearance of crystalline HfO_2 in Fig. 1a looking left to right, as the as-deposited film thickness increases from 5nm to 20nm. XTEM also demonstrates developing crystallinity in the thin films as a function of annealing temperature (comparing Figs. 1a – 1f). It is clear that several crystal orientations of HfO_2 occur from sample-to-sample and for the same sample in each micrograph, i.e., the HfO_2 films are polycrystalline. Fast Fourier Transform analysis was carried out on each XTEM micrograph in order to identify preferential crystal orientations. Fig. 2 provides two examples, the first (Fig. 2a) for the amorphous 5nm as-deposited film, which gives a somewhat 'fuzzy' Fourier image. In Fig. 2b – for the 10nm film annealed at 325^{o}C – bright spots appear in the FFT of the crystalline region and match well to some of the interplanar (d-) spacings of monoclinic HfO_2. In order of intensity (brightness) the d-spacings correlate to the following monoclinic (M) HfO_2 crystal orientations, -1 1 1, 0 0 2, 1 1 1, -2 1 1 and 1 0 0.

Although the micrographs capture only a small volume of the hafnia film, it is evident – comparing for example, Fig. 1b with Fig. 1e, that the average grain size of the polycrystalline material increases with elevated annealing temperature. This finding is explored in greater depth in the following paragraphs.

Grazing incidence X-ray diffraction measurements were carried out to extend the study of crystallinity. The surface of each sample was positioned with a 0.5^{o} offset to the incident X-ray beam ($\omega = 0.5^{o}$) and the detector (2θ) was scanned through the angular range 20^{o}-80^{o}. Fig. 3 presents diffraction data for two 20nm samples annealed at 475^{o}C / 625^{o}C for 1 min in flowing nitrogen, and one sample left as-deposited. Within Fig. 3 the expected diffraction peak positions [5] for orthorhombic and monoclinic phases of HfO_2 are indicated, labeled with the associated diffraction planes where the peak is expected to be prominent. For ease of comparison with Fig. 2, crystal planes evident in the XTEM are marked with an asterisk. XRD demonstrates there is little evidence of orthorhombic HfO_2 and that monoclinic HfO_2 develops in the samples fabricated here. Numerous peaks from the monoclinic phase are present, indicating that this phase is polycrystalline. Most prominent peaks are -1 1 1, 0 0 2, 1 1 1, 0 2 2, 0 1 1 and -2 1 1, respectively. This is in very close agreement with the crystal d-spacings extracted from XTEM analysis. Similarly the diffraction peak intensity is seen to increase as a function of annealing temperature. The most highly crystalline films are the thicker samples annealed at the highest temperature 625^{o}C. That said, there is some evidence of crystallinity in the as-deposited film.

Despite being thickness and temperature dependent, Fig. 4 illustrates that the crystallization of HfO_2 is only very weakly dependent on annealing time. Here the intensity of the -1 1 1 monoclinic HfO_2 XRD peak is used as a metric of crystallinity to compare different annealing conditions for the 20nm films [6]. The intensity of the -1 1 1 peak for each sample is plotted as a function of average crystallite diameter. This value was extracted using the Scherrer formula [7]. Crystallite size was estimated using $L = 0.9\lambda/\Delta 2\theta.\cos\theta_B$ where L is the structural coherence length (crystallite size), λ is the wavelength of the X-ray radiation, θ_B is the Bragg angle of the peak, and $\Delta 2\theta$ is the line broadening at half the X-ray peak intensity. There is a clear correlation between the XRD intensity and the crystallite diameter with both showing a distinct increase as a function of annealing temperature. For example, the average crystallite diameter in the 20nm as-grown hafnia film is ~6nm, and grows to ~10nm on average, for annealing at 475^{o}C, and to ~14nm for annealing at 625^{o}C. Visual comparison with the XTEM results in Fig. 1, shows the two data sets to be in close agreement. In contrast, annealing time does not significantly alter either the peak intensity or average crystallite diameter at any of the chosen annealing temperatures. This is particularly evident for samples annealed at 475^{o}C, where there is almost no difference in the HfO_2 crystal structure whether a sample is post-annealed for 1 min or for as long as 6 hrs.

From the point-of-view of future CMOS technologies utilizing HfO_2-based gate dielectrics, we find that the crystallization behavior of post-annealed HfO_2 on GaAs is almost completely analogous to the behavior of HfO_2 deposited on Si, as evidenced by the close agreement between our findings and the consensus of data from numerous studies of hafnia on Si [6, 8-10].

ii) Thickness and density

For each of the ALD-HfO_2 samples, film thickness and density was extracted using XRR measurements. In Fig. 5 an example XRR spectrum is presented for a 20nm film annealed at 325^{o}C for 1 min, alongside an optimized simulation of the sample structure from modelling. A close correlation is evident between the experimental data and the model used to extract film characteristics.

Fig. 6 summarizes the XRR thickness findings of the samples by relating measured film thickness to post-annealing temperature (for 1 min). The thickness of each of the as-deposited films (deposition temperature: 250^{o}C) is close to the nominal growth thickness of 5nm, 10nm or 20nm. Following post-annealing at 325^{o}C – and more so at 400^{o}C – each of the HfO_2 layers decreases in thickness by between 1-4%. Since XTEM and XRD have shown that post-annealing causes crystallization of the hafnia, this layer shrinking is most likely due to an associated compacting of the layer. Interestingly for samples post-annealed at 475^{o}C, this shrinkage is less than might be expected almost as if the layer increases in thickness as the temperature is raised from 400^{o}C to 475^{o}C. This trend is apparent in all three graphs of Fig. 6, independent of the as-deposited hafnia thickness. The trend is different to the case for HfO_2 on Si, where a continuous shrinking of the hafnia layer was seen as a function of annealing temperature [9].

In Fig. 7 a similar summary is presented, this time considering the HfO_2 density, also extracted from XRR. Again, all film densities are close to the nominal density of HfO_2 – 9.67 g/cm^3 [11]. Trends in the hafnia density closely mirror the trends in thickness in Fig. 6. For example, as the annealing temperature is raised to 325^{o}C and through 400^{o}C, the film density increases, further suggesting that the film is crystallizing. Again the samples annealed at 475^{o}C show a difference, i.e. a decrease in film density is apparent at this higher post-annealing temperature. A further discussion of this behavior at 475^{o}C is dealt with in section iv.

iii) Refractive index, dielectric constant and band gap

Ellipsometry was used to extract the refractive index for each of the fabricated samples. This was done by setting the HfO_2 layer thickness equal to that measured using XRR and then modelling the HfO_2 layer as a Cauchy layer [12]. Refractive index, n, was extracted from the model using the Cauchy formula $n(E) = A + BE^2 + CE^4$, and the Urbach expression $k = k_0 \exp(k_1 E)$, where A, B, C, k_0 and k_1 are fitting parameters and E is photon energy. From refractive index data, information about the dielectric constant, κ, of each hafnia film can be inferred, since $\kappa_{electron}$ – the electronic component of refractive index – is proportional to the square of the refractive index. The complete dielectric constant however, is equal to $\kappa_{electron} + \kappa_{lattice}$ – the lattice component – and for high-κ materials there is a dominant lattice contribution [13]. Therefore $\kappa_{electron}$ values are gross underestimates of the complete κ, but trends are indicative nonetheless. $\kappa_{electron}$ values are plotted in Fig. 8. Across hafnia films of all three nominal thicknesses some small increases in $\kappa_{electron}$ value are seen as a

function of post-annealing temperature following annealing at 325°C and 400°C. An exception exists for annealing at 475°C where $\kappa_{electron}$ is consistently lower for the highest annealing temperature.

The optical band gap of each high-κ film was extracted by applying the Wemple - di Domenico treatment to each data set [14]. Here $(n^2 - 1)^{-1}$ was plotted as a function of E^2 and the gradient of the straight line plot was used to infer band gap. Scientific literature suggests that the HfO_2 band gap varies in the range 5.4-6.0 eV and is expected to increase as the hafnia density increases [9]. Fig. 9 demonstrates that indeed the band gaps inferred in this study do replicate the trends in density extracted from XRR. Despite the slightly unexplained behaviour we have seen for samples annealed at 475°C, within the error bar of this analysis, all but one of the band gaps fall within the accepted range of 5.4-6.0 eV. The exception is the 20nm HfO_2 film annealed at 475°C which has a band gap lower than expected, closer to 5 eV.

iv) Issues following high-temperature (475°C) post-annealing

In order to further investigate the sample properties after annealing at 475°C, XPS was employed. Although the 20nm hafnia sample displayed the most anomalous behavior under examination by XRR and ellipsometry, the surface sensitivity of XPS would only allow investigation of the uppermost HfO_2 surface. Therefore, since the same trends – though less conspicuous – occurred independent of thickness, XPS was carried out on the 5nm samples in order to investigate the entire hafnia layer. XPS was carried out on all 5nm samples as a function of annealing temperature, with particular focus on the As 3d peak, as displayed in Fig. 10.

For the as-deposited sample and those annealed at 325°C and 400°C, a prominent peak appears at 40-41eV with evidence of a slight shoulder at higher binding energies. For the sample annealed at 475°C the As 3d peak is accompanied by a further peak at ~44eV. Modeling of the experimental data suggests this additional peak is symptomatic of As-oxide formation. SIMS depth profiling was carried out to monitor the elemental profile of oxygen, gallium and arsenic in the 20nm samples as a function of annealing conditions, as presented in Fig. 11. As expected, the oxygen depth profile is similar for all four samples under investigation, showing a near constant concentration from the surface to a depth of ~23nm, before quickly trailing off. Some slight evidence of oxygen diffusion into the GaAs bulk is apparent as the post-annealing temperature is raised, though this effect is small. In contrast, the gallium concentration is negligible in the 15nm closest to the sample surface, rising slightly closer to the HfO_2 / GaAs interface, before rising sharply in concentration close to the GaAs substrate. For all four annealing conditions the gallium depth profile is almost identical. For the as-deposited sample and those annealed at 325°C and 400°C, the arsenic depth profile is comparable to the gallium profile, though the concentration rise close to the HfO_2 / GaAs interface is less abrupt. Both Ga and As diffuse into the hafnia layer but the As appears to do so at a faster rate and possibly by a different diffusion mechanism. As diffusion is most significant for the sample annealed at 475°C, where the presence of As is significantly higher at depths <23nm, i.e. within the HfO_2 film. The presence of As in the film supports the possibility of As-oxide formation as suggested by XPS. Furthermore, since the band gap of As-oxide is ~5eV [15], the incorporation of As-oxide within the hafnia layer is consistent with the findings from ellipsometry on this sample.

In addition to consistency with band gap analysis, the formation of As-oxide within the hafnia layer would also explain the other inconsistent data points from earlier experimental discussions. For example, XRR showed that the layer thickness was increasing after annealing at 475^{o}C. This is consistent with As-oxide forming in the HfO_2 layer due to As diffusion from the GaAs substrate, causing a small swelling of the layer. Likewise XRR showed an accompanying density decrease. This is consistent with incorporation of As-oxide in the HfO_2, which has a density of 3.74g/cm^3 [16] compared to 9.67g/cm^3 for HfO_2. A question remains as to the exact nature of the As-oxide, since XTEM shows no obvious interlayer. Similarly, XRR modeling was best optimized with no As-oxide interlayer present. It therefore seems likely that 'pockets' of this oxide are incorporated within the hafnia layer and that it does not form a distinct interlayer.

Interestingly an earlier study on the topic of post-annealing of atomic-layer-deposited HfO_2 on GaAs also found the hafnia film properties to be influenced by the formation of a secondary oxide after post-annealing [17]. The study by Kim *et al.* is similar to our own, but focused on post-annealing at higher temperatures. Some comparable conclusions were deduced in that developing HfO_2 crystallization following post-annealing was accompanied by a decreasing hafnia band gap at high annealing temperatures. The major difference between this current study and the findings of Kim *et al.*, is that their results clearly showed a Ga oxide to be responsible, rather than an As oxide. This was demonstrated by near-edge X-ray adsorption fine structure and corroborated by XPS. Since those results are concerned with post-annealing at 600^{o}C and 700^{o}C, rather than at the relatively lower temperatures of 325^{o}C - 475^{o}C, though seemingly unlikely, it could be that Ga diffusion becomes more prevalent than As at higher temperatures. More likely however is that variances arise due to critical differences introduced by the GaAs substrate and the treatment prior to ALD. Our study used an epitaxial film of very high quality compared to commercial GaAs substrates. The second difference, which could be the most significant, is that our GaAs surface was not exposed to any chemical or other treatment prior to ALD and was combined with a fast transfer (<1min) in N_2 ambient from the MOVPE glove box to the ALD chamber. Kim *et al.*'s samples were submerged in a buffered-oxide etch for 20 min before ALD which could dramatically change the starting surface [18]. For example, if a Ga-rich surface were formed, this could explain the additional up-diffusion of Ga during post-annealing.

Conclusions

The effects of post-annealing conditions on solid-phase crystallisation of atomic-layer-deposited HfO_2 films grown on GaAs have been investigated. Particular focus was given to preferential crystal orientation / crystallite size, and changes in film thickness / density / permittivity / optical band gap as a function of annealing conditions. Following thermal processing in nitrogen ambient at temperatures from 325^{o}C to 475°C, the initially produced amorphous/partially crystallized HfO_2 films changed into a well-ordered polycrystalline structure with no detectable interfacial layer between the film and the GaAs substrate. Though hafnia properties were predictable and similar to those of HfO_2 on Si for low temperature processing, in the case of annealing at 475°C, the thickness of the film was relatively increased compared to that of an as-grown film, and displayed unexpected film characteristics. Films were seen to demonstrate a decrease in density, permittivity and band gap.

XPS, band gap analysis and the up-diffusion of As in SIMS depth profile data indicated that As oxide is formed within the HfO_2 film during annealing at 475°C. In a past study, the formation of oxide in the hafnia film, resulting from the underlying substrate, had been previously noted, however Ga oxide and not As oxide was found to be present. Differences are believed to arise because of variances introduced by the different GaAs substrate quality and GaAs surface treatment prior to ALD.

Acknowledgements

This work was part of the EU MATERA ERA-NET project: Epitaxial Nanostructured GaAs on Si for Next Generation Electronics (ENGAGE: IR-2008-0006). Enterprise Ireland is acknowledged for the financial support. The authors would like to thank Dr Kevin Thomas for the MOVPE growth, Alan Blake (Tyndall Central Fabrication Facilities) for the ALD films and Dr Patrick Carolan for the sample preparation and TEM images. PMN acknowledges the support of Science Foundation Ireland's Strategic Research Cluster Programme ("Precision" 08/SRC/I1411), the Irish Higher Education Authority INSPIRE programme, funded by the Irish Government's Programme for Research in Third Level Institutions, Cycle 5, National Development Plan 2007-2013.

References

[1] G. D. Wilk, R. M. Wallace and J. M. Anthony, High-κ gate dielectrics: Current status and materials properties considerations, J. Appl. Phys. 89 (2001) 5243.

[2] D. Ceresoli and D. Vanderbilt, Structural and dielectric properties of amorphous ZrO_2 and HfO_2, Phys. Rev. B 74 (2006) 125108.

[3] ImageJ software, version 1.46n; T. J. Collins, ImageJ for microscopy, BioTechniques 43(1) (2007) 25.

[4] Bede REFS 4.0 software; M. Wormington, D. K. Bowen and B. K. Tanner, Principles And Performance Of A Pc-based Program For Simulation Of Grazing-incidence X-ray Reflectivity Profiles, Mater. Res. Soc. Symp. Proc. 238 (1992) 119.

[5] International Centre for Diffraction Data 1999 JCPDS Powder Diffraction, File Nos. 34-104 and 43-107.

[6] M.-Y. Ho, H. Gong, G. D. Wilk, B. W. Busch, M. L. Green, P. M. Voyles, D. A. Muller, M. Bude, W. H. Lin, A. See, M. E. Loomans, S. K. Lahiri and Petri I. Räisänen, Morphology and crystallization kinetics in HfO_2 thin films grown by atomic layer deposition, J. Appl. Phys. 93 (2003) 1477.

[7] P. Scherrer, Nachrichten von der Gesellschaft der Wissenschaften zu Göttingen, Mathematisch-Physikalische Klasse 1918 (1918) 98.

[8] S. Toyoda, J. Okabayashi, H. Kumigashira, M. Oshima, K. Yamashita, M. Niwa, K. Usuda and G. L. Liu, Crystallization in HfO_2 gate insulators with in situ annealing studied by valence-band photoemission and x-ray absorption spectroscopy, J. Appl. Phys. 97 (2005) 104507.

[9] M. Modreanu, J. Sancho-Parramon, D. O'Connell, J. Justice, O. Durand, B. Servet, Solid phase crystallisation of HfO_2 thin films, Mater. Sci. Eng. B 118 (2005) 127.

[10] M. Modreanu, J. Sancho-Parramon, O. Durand, B. Servet, M. Stchakovsky, C. Eypert, C. Naudin, A. Knowles, F. Bridou, M.-F. Ravet, Investigation of thermal annealing effects on microstructural and optical properties of HfO2 thin films, Appl. Surf. Sci. 253 (2006) 328.

[11] P. D. Kirsch, M. A. Quevedo-Lopez, H. -J. Li, Y. Senzaki, J. J. Peterson, S. C. Song, S. A. Krishnan, N. Moumen, J. Barnett, G. Bersuker, P. Y. Hung, B. H. Lee, T. Lafford, Q. Wang, D. Gay and J. G. Ekerdt, Nucleation and growth study of atomic layer deposited HfO_2 gate dielectrics resulting in improved scaling and electron mobility, J. Appl. Phys. 99 (2006) 023508.

[12] F. A. Jenkins and H. E. White, Fundamentals of Optics, fourth ed., McGraw-Hill, Inc., 1981, pp. 482.

[13] J. Robertson, High dielectric constant oxides, Eur. Phys. J. Appl. Phys. 28 (2004) 265.

[14] S. H. Wemple and M. DiDomenico Jr., Behavior of the Electronic Dielectric Constant in Covalent and Ionic Materials, Phys. Rev. B 3 (1971) 1338.

[15] S. W. McKnight, E. D. Palik and T. N. Bhar, Cathodoluminescence studies of anodic oxides on GaAs, J. Vac. Sci. Tech. 17(5) (1980) 967.

[16] D. L .Perry, Handbook of Inorganic Compounds, second ed., CRC Press, Taylor & Francis Group FL, 2011, pp. 43.

[17] C. Y. Kim, S. W. Cho, M.-H. Cho, K. B. Chung, D. C. Suh, D.-H. Ko, C.-H. An, H. Kim and H. J. Lee, Changes in the structure of an atomic-layer-deposited HfO_2 film on a GaAs (100) substrate as a function of postannealing temperature, Appl. Phys. Lett. 95 (2009) 042903.

[18] S. Adachi and D. Kikuchi, Chemical Etching Characteristics of GaAs (100) Surfaces in Aqueous HF Solutions, J. Electrochem. Soc. 147(12) (2000) 4618.

Figure captions

Fig. 1. Cross-sectional electron microscope images showing (a) as-deposited HfO_2 films of thickness 5nm, 10nm, 20nm, respectively, looking from left to right, (b) films annealed at 325°C for 60s, (c) films annealed at 400°C for 60s, (d) films annealed at 475°C for 60s, (e) 20nm film annealed at 550°C for 60s and (f) 20nm film annealed at 625°C for 60s.

Fig. 2. Cross-sectional electron microscope images with accompanying Fast Fourier Transform analysis for (a) an amorphous 5nm as-deposited HfO_2 film and (b) a crystalline 10nm film annealed at 325°C for 60s.

Fig. 3. Grazing incidence X-ray diffraction data for 20nm HfO_2 samples annealed for 60s at 475°C (black), 625°C (red), or left as-deposited (blue). Expected diffraction peak positions for orthorhombic and monoclinic phases of HfO_2 are indicated and labeled.

Fig. 4. Intensity of the -1 1 1 monoclinic HfO_2 peak from grazing incidence X-ray diffraction plotted as a function of average HfO_2 crystallite diameter for various annealing conditions on the 20nm films. This value was extracted using the Scherrer formula.

Fig. 5. X-ray reflectivity data (black) for a 20nm HfO_2 film annealed at 325°C for 1 min, alongside a simulated version (red) from a model of the sample structure.

Fig. 6. HfO_2 thickness extracted from X-ray reflectivity as a function of annealing conditions for films of nominal as-deposited thickness of (a) 5nm, (b) 10nm, and (c) 20nm. Nominal thickness is marked by dashed lines.

Fig. 7. HfO_2 density extracted from X-ray reflectivity as a function of annealing conditions for films of as-deposited thickness (a) 5nm, (b) 10nm, and (c) 20nm. Nominal density is marked by dashed lines.

Fig. 8. Electronic component of the HfO_2 dielectric constant, extracted from X-ray reflectivity and ellipsometry, as a function of photon energy and annealing conditions for films of nominal as-deposited thickness (a) 5nm, (b) 10nm, and (c) 20nm.

Fig. 9. HfO_2 band gap extracted from X-ray reflectivity and ellipsometry as a function of annealing conditions for films of nominal thickness (a) 5nm, (b) 10nm, and (c) 20nm. Bounds for the band gap values are indicated by the shaded regions.

Fig. 10. X-ray photoelectron spectroscopy showing the As 3d peak for 5nm HfO_2 films exposed to various annealing conditions (left) and modeled fits to the experimental data for the additional peak(s) seen in the sample annealed at 475°C (right).

Fig. 11. Secondary-ion mass spectrometry depth profiles for (a) oxygen, (b) gallium and (c) arsenic, for 20nm HfO_2 films after annealing at various temperatures.

Figures (if any)

Click here to download Figures (if any): Figure 1.pdf

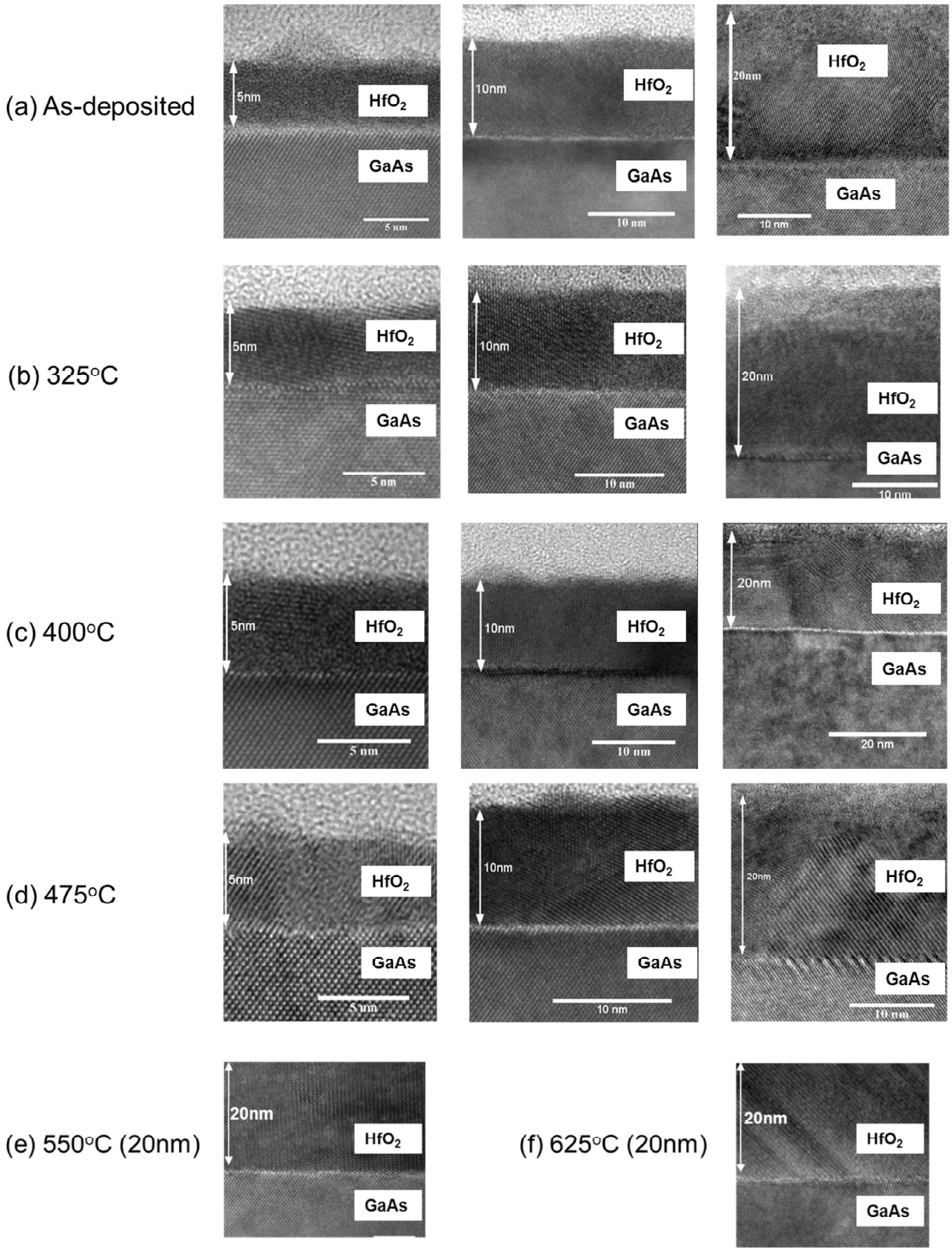

(Fig.1)

Figures (if any)
Click here to download Figures (if any): Figure 2.pdf

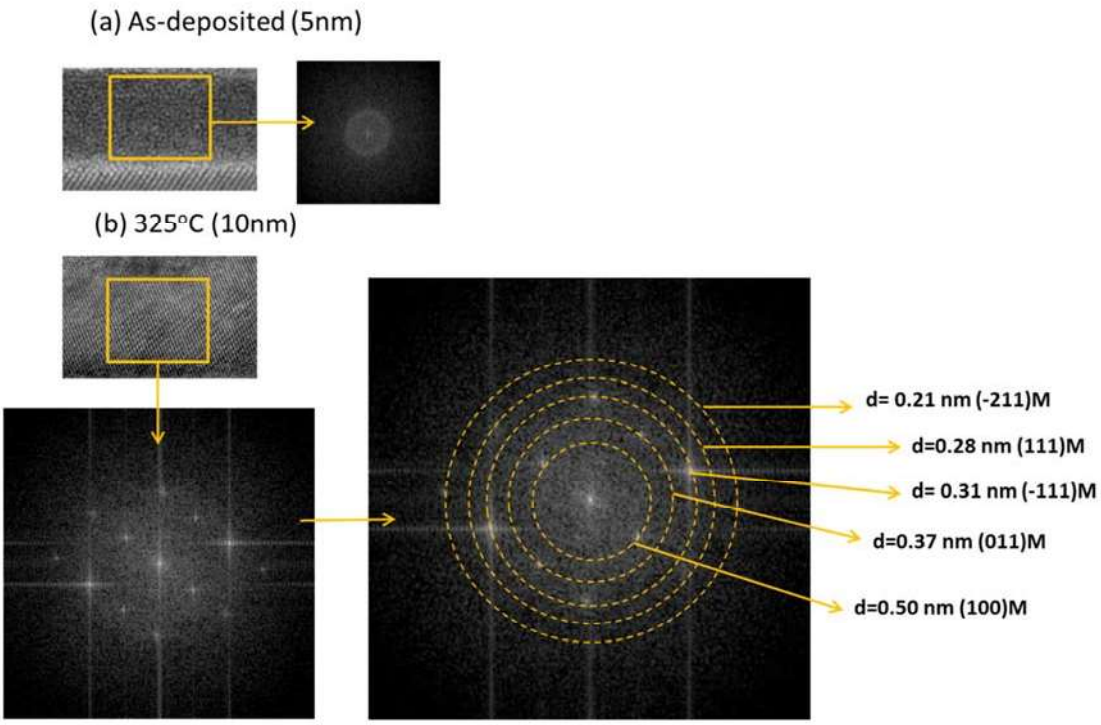

(Fig. 2)

Figures (if any)
Click here to download Figures (if any): Figure 3.pdf

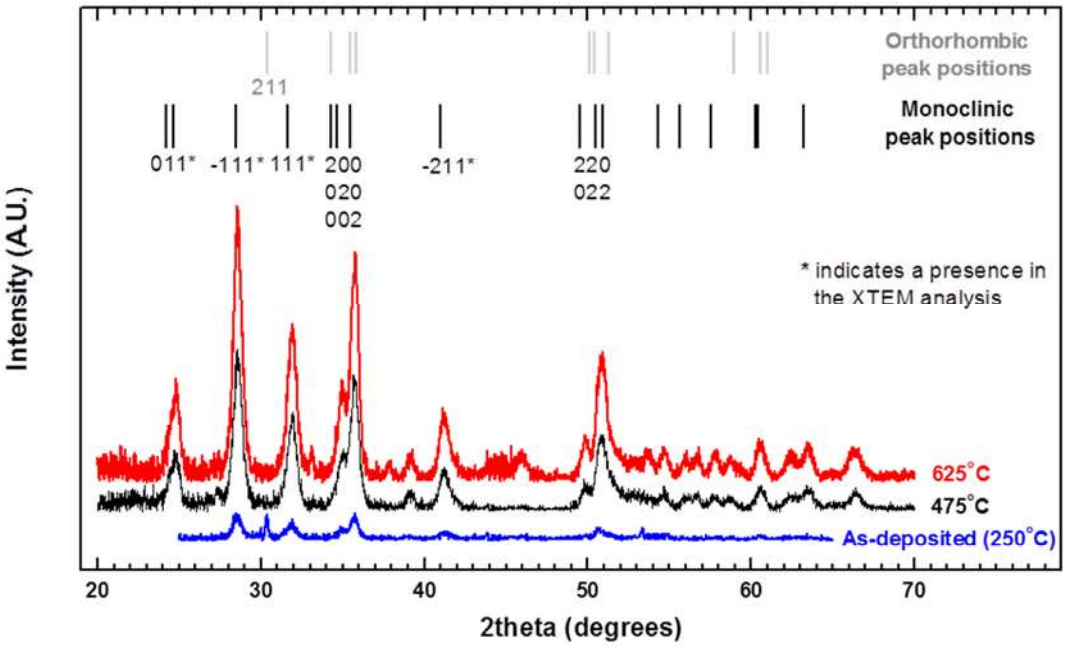

(Fig. 3)

Figures (if any)
Click here to download Figures (if any): Figure 4.pdf

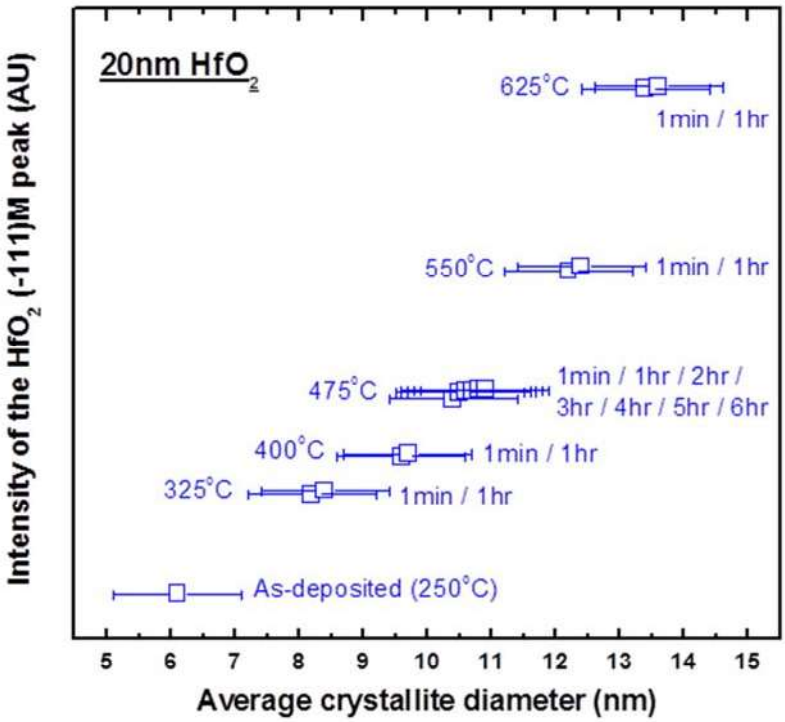

(Fig. 4)

Figures (if any)

Click here to download Figures (if any): Figure 5.pdf

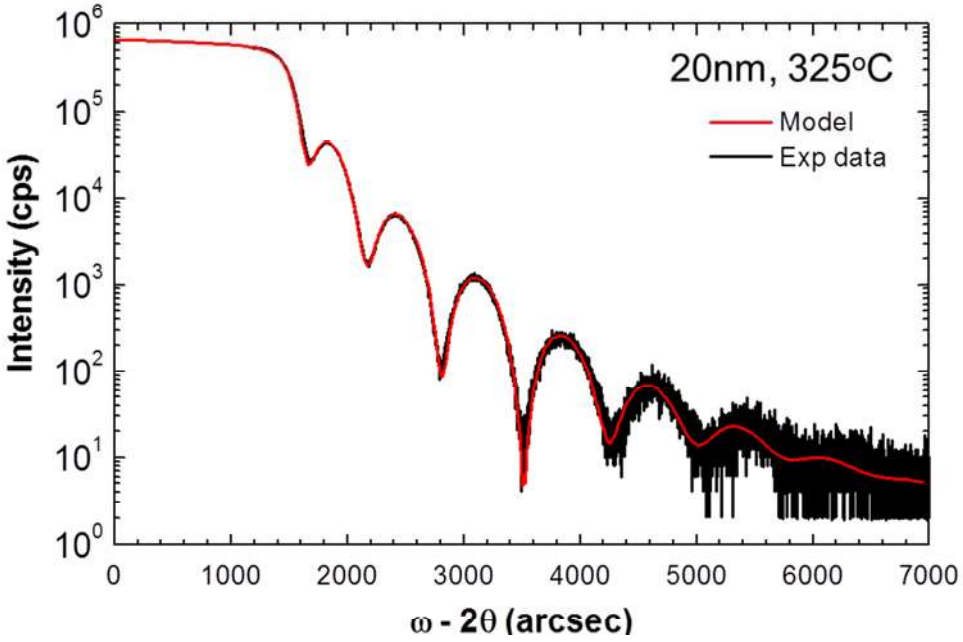

(Fig. 5)

Figures (if any)
Click here to download Figures (if any): Figure 6.pdf

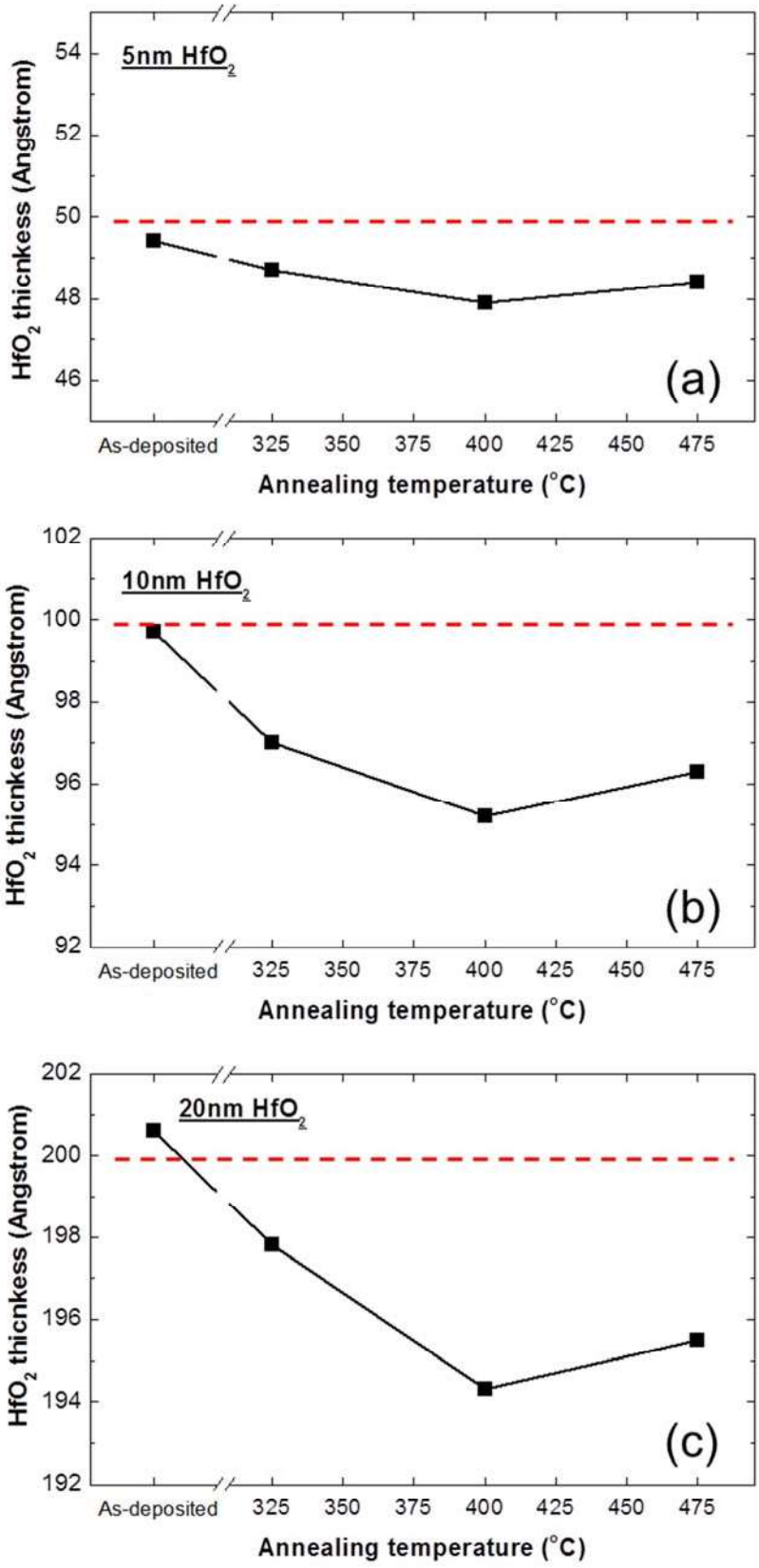

(Fig. 6)

Figures (if any)

Click here to download Figures (if any): Figure 7.pdf

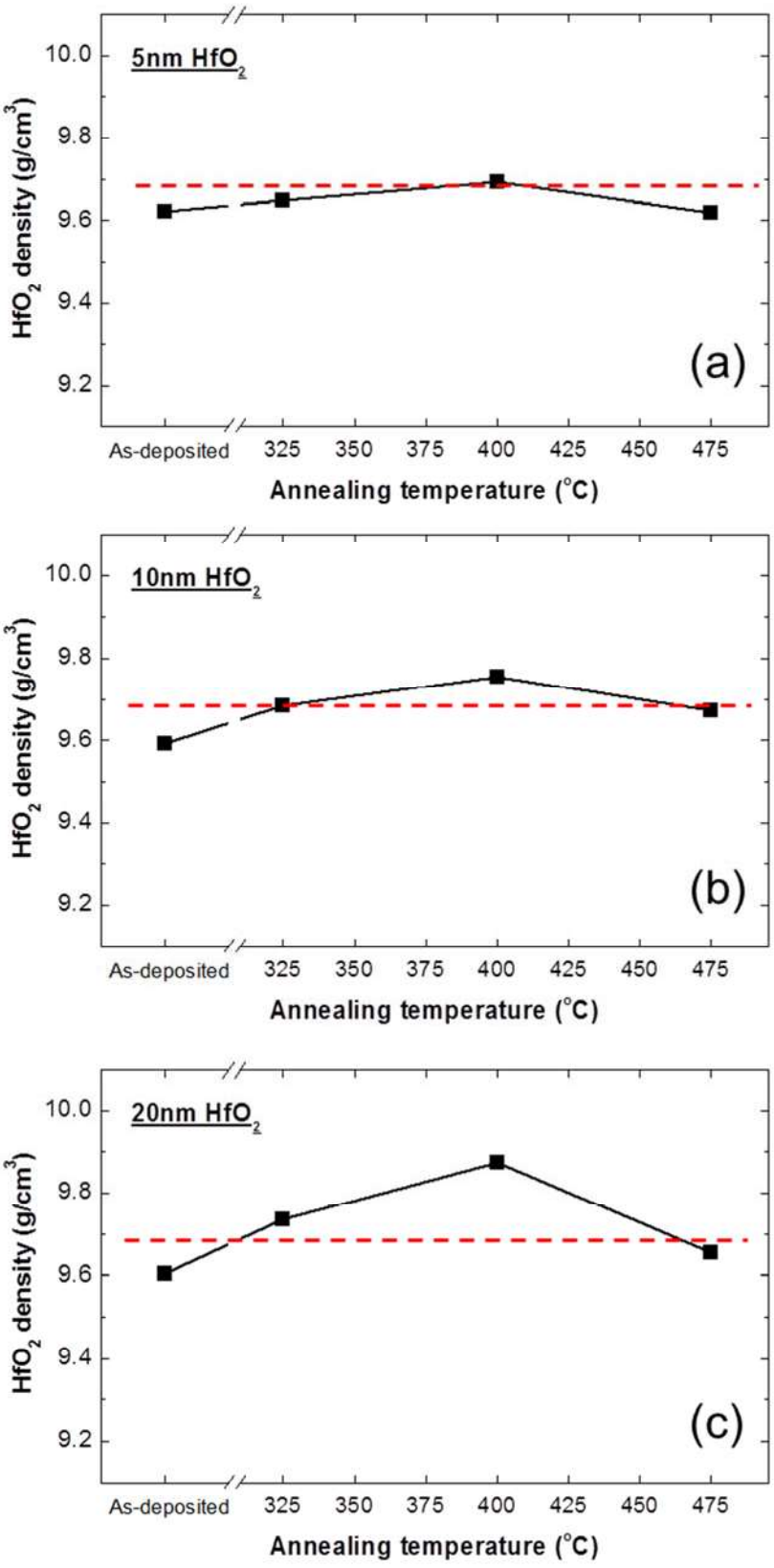

(Fig. 7)

Figures (if any)

Click here to download Figures (if any): Figure 8.pdf

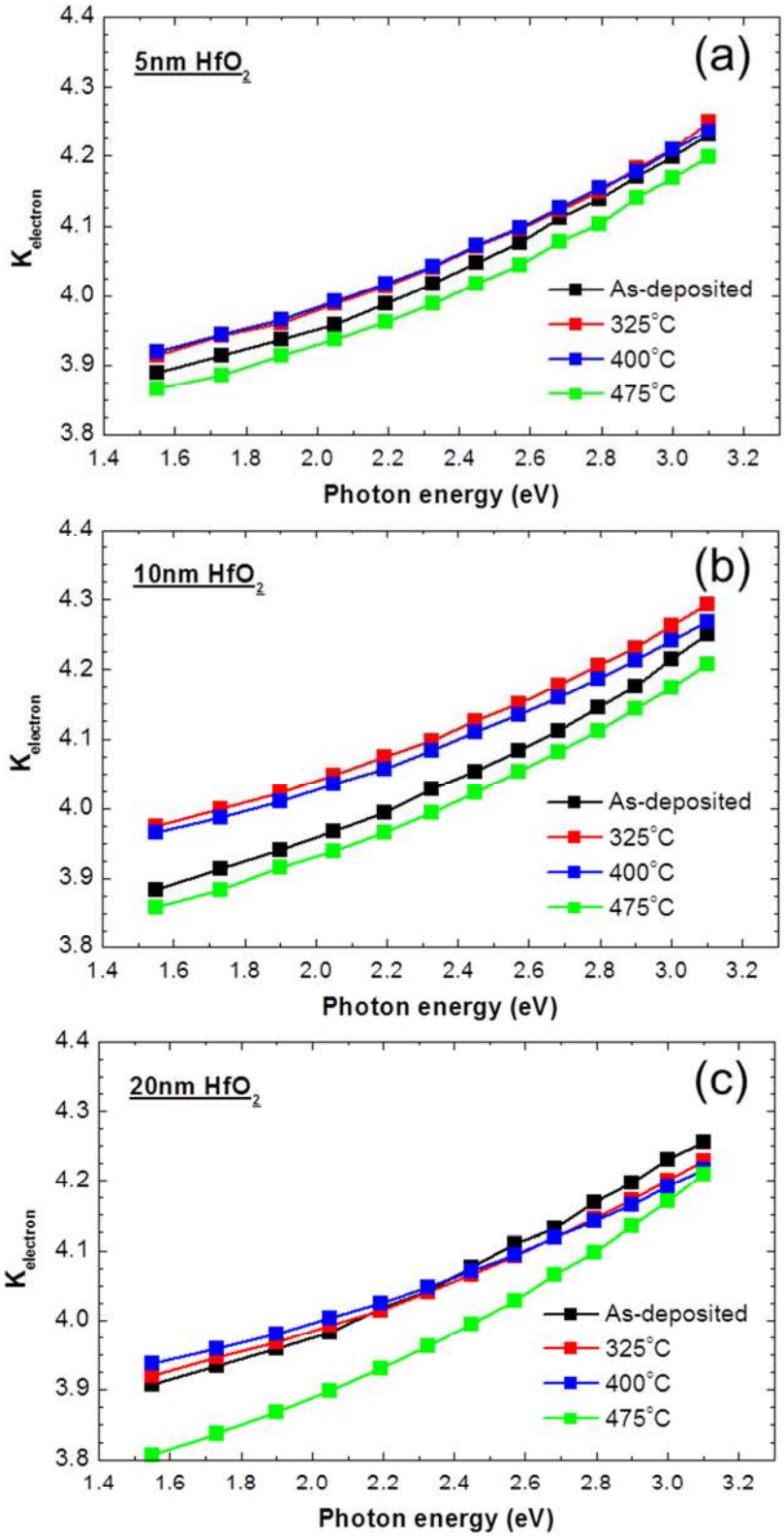

(Fig. 8)

Figures (if any)

Click here to download Figures (if any): Figure 9.pdf

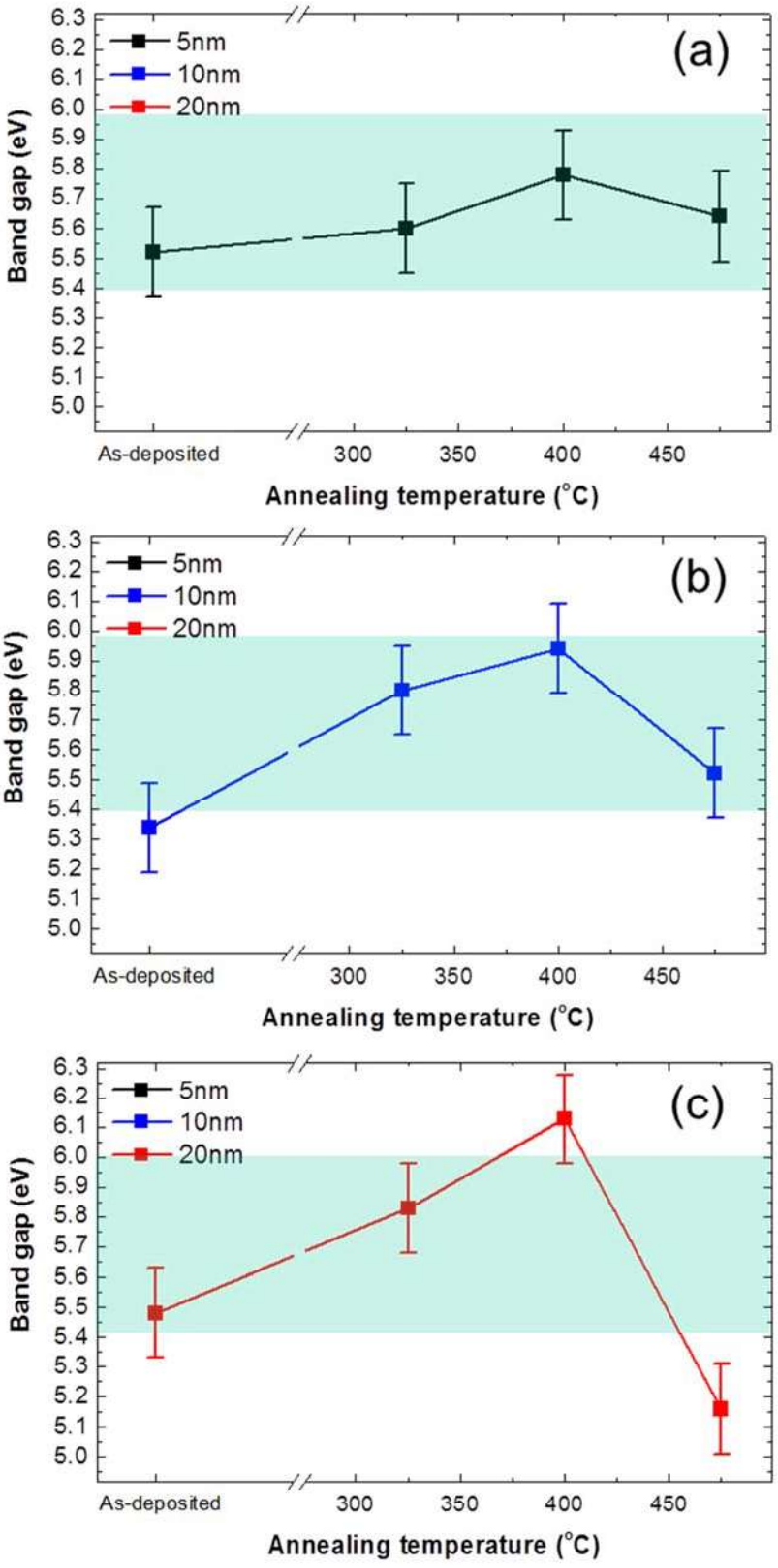

(Fig. 9)

Figures (if any)
Click here to download Figures (if any): Figure 10.pdf

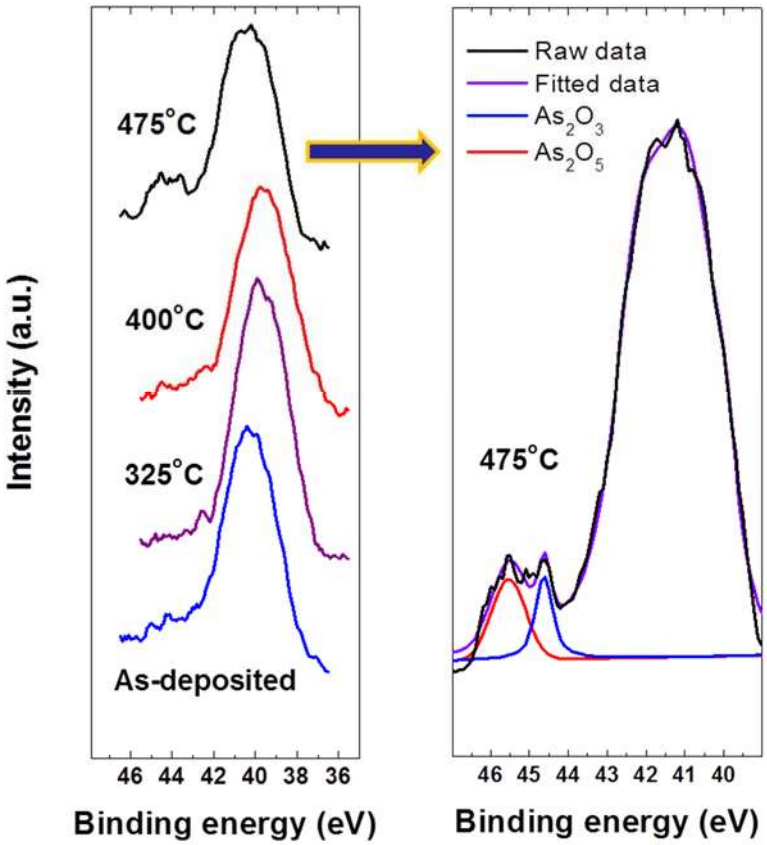

(Fig. 10)

Figures (if any)

Click here to download Figures (if any): Figure 11.pdf

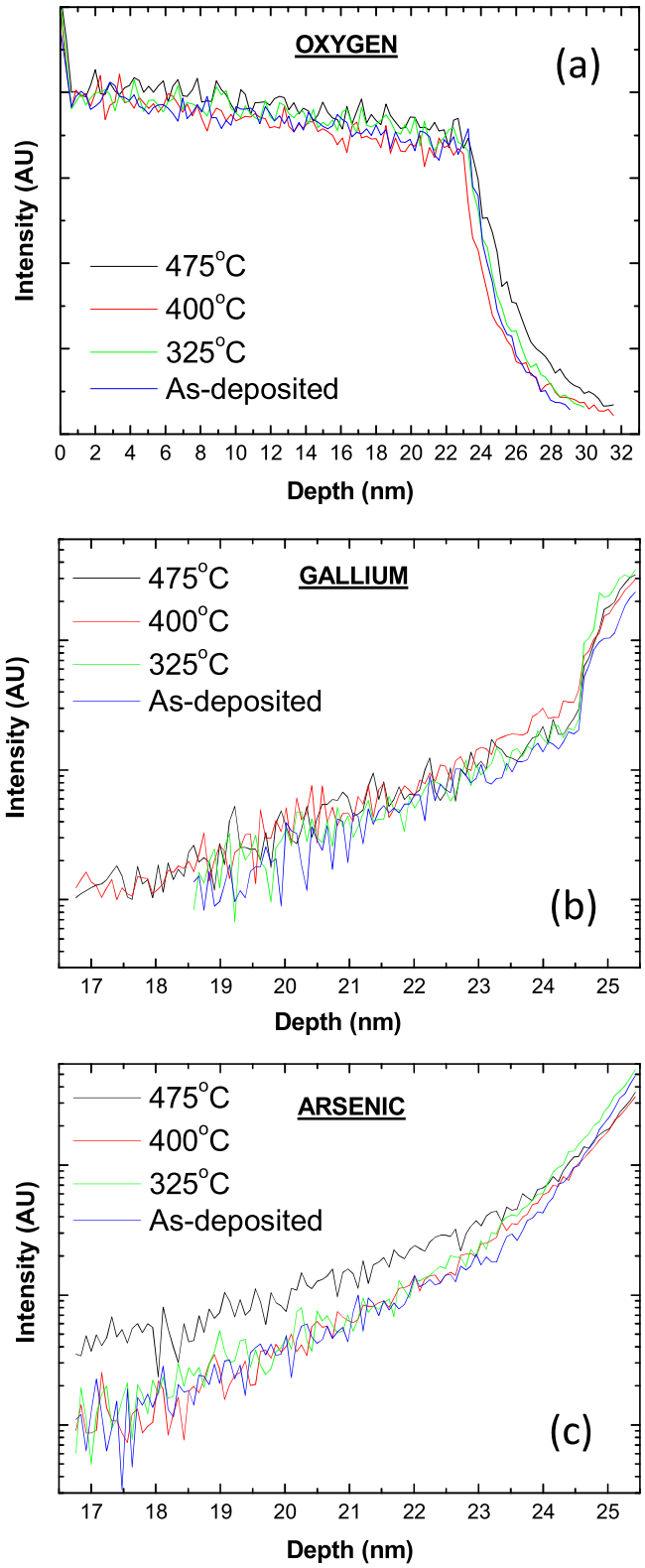

(Fig. 11)